minerals

MDPI

Article

Trace-Element Fractionation and Aqueous Release in Serbian FGD Gypsum: A Comparative Study of Three Materials

Ivana Vulović [1], Sandra Petković Papalazarou [1,*], Jelena Isailović [1], Ljiljana Matović [2], Tingfeng Liu [3], Wenyi Tan [3] and Srećko Stopić [4,*]

[1] Mining Institute Belgrade, Batajnički put 2, 11080 Belgrade, Serbia; ivana.vulovic@ribeograd.ac.rs (I.V.); jelena.isailovic@ribeograd.ac.rs (J.I.)
[2] Vinča Institute of Nuclear Sciences, National Institute of the Republic of Serbia, University of Belgrade, Mike Petrovića Alasa 12-14, Vinča, 11000 Belgrade, Serbia; ljiljam@vin.bg.ac.rs
[3] School of Environment Engineering, Nanjing Institute of Technology, Nanjing 211167, China; hjliutingfeng@njit.edu.cn (T.L.); twy1102@gmail.com (W.T.)
[4] IME Process Metallurgy and Metal Recycling, RWTH Aachen University, 52056 Aachen, Germany
* Correspondence: sandra.petkovic@ribeograd.ac.rs (S.P.P.); sstopic@metallurgie.rwth-aachen.de (S.S.)

Abstract

Flue gas desulfurization (FGD) gypsum is increasingly considered a secondary raw material, but gypsum purity and bulk mineralogy alone do not fully describe the environmental behavior of associated trace elements. Three Serbian FGD gypsum materials were investigated: FGD-A and FGD-B from two wet-FGD operating streams of the Nikola Tesla A Thermal Power Plant and FGD-C from Kostolac B. Bulk characterization, X-ray diffraction, sequential extraction, and aqueous leaching were combined. FGD-A and FGD-B contained >98.6 wt.% $CaSO_4{\cdot}2H_2O$, whereas FGD-C contained 87.47–92.06 wt.%; gypsum nevertheless remained the predominant crystalline phase in all three materials. Operationally defined non-residual fractions (F1–F3) accounted for 74.4%–82.8% of As, 91.9%–95.4% of Cd, and 89.9%–96.8% of V, whereas 81.5%–88.3% of Sb was retained in the residual fraction. Aqueous release was generally low but element- and material-dependent: Zn reached 5.25 μg L^{-1} in FGD-B, V reached 0.98 μg L^{-1} in FGD-C, and Pb remained below the validated detection limit in all leachates. The non-residual fraction was not directly proportional to aqueous release, showing that sequential fractionation and water leaching provide complementary information. The results demonstrate that FGD gypsum materials with broadly similar gypsum-rich characteristics can nevertheless exhibit distinct trace-element partitioning and short-term aqueous release.

Keywords: FGD gypsum; trace elements; sequential extraction; aqueous leaching; X-ray diffraction; geochemical stability; waste valorization

Check for updates

Academic Editor: Andrey G. Kalinichev

Received: 25 September 2026
Revised: 14 October 2026
Accepted: 18 October 2026
Published: 20 October 2026

Copyright: © 2026 by the authors. Licensee MDPI, Basel, Switzerland. This article is an open access article distributed under the terms and conditions of the Creative Commons Attribution (CC BY) license.

1. Introduction

Wet limestone flue gas desulfurization (FGD) is one of the most widely applied technologies for controlling SO_2 emissions from coal-fired power plants. In this process, SO_2 is absorbed into a Ca-bearing slurry produced from limestone, followed by oxidation of sulfite species and crystallization of calcium sulfate dihydrate ($CaSO_4{\cdot}2H_2O$) as the principal solid by-product [1,2]. The resulting FGD gypsum is generally characterized by a high gypsum content, although its composition and impurity burden depend on the properties of the coal and limestone feedstocks, particulate carry-over, process-water chemistry, and operating conditions of the individual FGD system [1,3]. Because large quantities of this Ca-rich

secondary material are generated worldwide, management strategies have progressively shifted from disposal toward beneficial use and circular-resource utilization [3–5].

Conventional utilization routes include gypsum-based construction products, cement manufacture, and agricultural soil amendment [3–5]. More recently, research has increasingly focused on higher-value applications and processes capable of exploiting the $CaSO_4$ matrix as a reactive secondary mineral resource. FGD gypsum has been investigated as a sulfate activator in low-clinker cementitious systems [6], converted into high-strength α-calcium sulfate hemihydrate [7], and used as a calcium source for the preparation of precipitated or nano-$CaCO_3$ through CO_2 mineralization [8–11]. Mineral impurities can affect $CaCO_3$ polymorphism during carbonation [12], while metallic impurities may influence carbonation efficiency and undergo redistribution during the process [13]. Carbonated products may consequently exhibit different trace-element retention and leaching behavior from the starting material [13]. These environmental aspects are increasingly evaluated together with technological, mechanical, and life-cycle performance during FGD-gypsum valorization [14].

However, technological suitability and high $CaSO_4 \cdot 2H_2O$ content do not necessarily imply equivalent environmental stability. Multi-plant investigations have demonstrated substantial variability in trace-element concentrations among FGD gypsum samples from different coal-fired power plants [15]. Chemical speciation and operational fractionation also vary among elements and materials, indicating that total concentration alone does not adequately describe potential environmental behavior [16,17]. Trace-element transfer from coal combustion and air-pollution-control systems can additionally contribute to differences among FGD-derived materials [18]. Arsenic provides a particularly clear example: a multi-sample study of coal-fired-power-plant FGD gypsum showed source-dependent concentrations and fractionation, predominant As(III) speciation, and greater release potential during prolonged leaching, demonstrating that short-term leaching alone may not fully describe its stability [19].

Sequential extraction is useful for differentiating operationally defined element pools. Classical sequential-extraction procedures were developed to distinguish fractions associated with progressively more resistant solid-phase components [20], and the BCR scheme was subsequently refined to improve operational reproducibility [21]. These fractions should nevertheless not be interpreted as direct measures of short-term aqueous mobility or bioavailability. Recent FGD-gypsum studies have shown that fractionation and leaching behavior are strongly element-dependent [22,23]. Direct leaching therefore provides complementary information, because constituent release from FGD gypsum is influenced by the applied water-contact conditions [24] and may differ under longer-term or alternative management scenarios [25].

Despite the growing literature on FGD gypsum characterization, valorization, and environmental behavior, most multi-sample studies have primarily focused on differences among power plants or geographical regions [15,23], whereas comparisons of trace-element behavior in gypsum materials originating from separately operated FGD lines within the same power plant remain relatively limited. Trace-element fractionation and direct aqueous release are also rarely evaluated together for the same broad suite of elements [22,23]. The specific contribution of the present study is therefore the integrated assessment of conventional FGD-gypsum quality, crystalline phase composition, operationally defined trace-element fractionation, and short-term aqueous release within a single analytical framework. This approach enables comparison between two independently operated FGD lines within the same power plant and a material from a second power plant, while directly examining whether operationally non-residual element fractions are reflected in aqueous release. Establishing the initial state of untreated FGD gypsum is also relevant

for subsequent treatment studies, because processes such as carbonation can modify trace-element partitioning and the properties of the resulting products [13].

Accordingly, this study investigates the physicochemical and mineralogical characteristics, trace-element fractionation, and aqueous leaching behavior of three FGD gypsum materials from Serbian coal-fired power plants. FGD-A and FGD-B originated from two investigated wet-FGD operating streams of the Nikola Tesla A Thermal Power Plant in Obrenovac, enabling a within-plant comparison, whereas FGD-C originated from Kostolac B and provides a between-plant comparison. The distributions of As, Cd, Cr, Pb, Cu, Ni, V, Zn, Sb, and Co among four operationally defined sequential-extraction fractions were compared with their short-term aqueous release. The study specifically examines whether gypsum-dominated materials exhibit comparable trace-element behavior, whether differences in trace-element behavior are observed between the investigated FGD materials originating from separately operated lines within the same power plant, and whether the operationally defined non-residual fraction is reflected proportionally in direct aqueous release. The resulting dataset also provides a baseline for future before–after investigations of treatments such as carbonation and mechanochemical processing.

2. Materials and Methods

2.1. FGD Gypsum Samples

Three flue gas desulfurization (FGD) gypsum materials generated at two Serbian lignite-fired thermal power plants were investigated and designated FGD-A, FGD-B, and FGD-C. FGD-A originated from the C1 wet-FGD system at the Nikola Tesla A Thermal Power Plant (Obrenovac, Serbia), treating flue gases from units A3 and A4, whereas FGD-B originated from the separately operated C2 system serving units A5 and A6. Both systems employ the wet limestone–gypsum process and use lignite from the Kolubara coal basin. FGD-C originated from the wet limestone–gypsum FGD system at the Kostolac B Thermal Power Plant, which uses lignite from the Drmno open-pit mine. The materials were collected during the corresponding performance-testing campaigns in June 2026 (FGD-A and FGD-B) and February 2026 (FGD-C). The sampling periods and selected operational characteristics documented for the investigated FGD installations are summarized in Table 1.

Table 1. Sampling information, fuel sources, and selected operating parameters of the investigated FGD systems.

Parameter	FGD-A	FGD-B	FGD-C
Thermal power plant	Nikola Tesla A	Nikola Tesla A	Kostolac B
FGD installation	Absorber C1	Absorber C2	B1 FGD system
Generating units	A3–A4	A5–A6	B1
FGD technology	Wet limestone–gypsum	Wet limestone–gypsum	Wet limestone–gypsum
Coal type and source	Kolubara lignite	Kolubara lignite	Drmno lignite
Sampling period	June 2026	June 2026	February 2026
Inlet SO_2 (mg/Nm^3)	1523.1–2818.1	3152.2–5265.6	5256.4–5692.9
Outlet SO_2 (mg/Nm^3)	16.5–68.5	139.4–193.9	30.4–70.6
SO_2 removal efficiency (%)	97.2–99.0	94.0–97.3	98.7–99.4
Outlet flue-gas temperature (°C)	65.2–65.7	65.3–66.4	63.4–64.5
Outlet particulate matter (mg/Nm^3)	10.6–15.5	9.1–15.4	9.8–11.7

Note: Ranges represent measurements during the respective performance-testing campaigns. SO_2 and particulate-matter concentrations refer to dry gas at 273.15 K and 101.3 kPa, normalized to 6% O_2. For FGD-A and FGD-B, inlet SO_2 values are reported averages of the corresponding two generating-unit inlet streams.

For each investigated FGD gypsum material, repeated time-resolved sampling was conducted during the corresponding industrial measurement campaign. Samples were collected at the discharge point of the vacuum-belt conveyor, immediately before the gypsum entered the storage silo. Access was provided through the chute door, and each sample was collected manually with a scoop across the full width of the moving belt to obtain a representative cross-sectional portion of the material. Approximately 1 kg of gypsum was collected during each sampling event. The collected samples were stored in closed PVC containers at room temperature until laboratory preparation and analysis. Three independent samples were collected at approximately evenly distributed time intervals during an 8 h period on each of two consecutive days, resulting in six independent field samples (n = 6) per investigated material, corresponding to 18 field samples in total.

The individual field samples were initially characterized separately for routine physicochemical and technological parameters. Subsequently, the six samples belonging to each FGD material were combined and homogenized to obtain one representative laboratory sample for FGD-A, FGD-B, and FGD-C, respectively. This representative material was used for the subsequent detailed laboratory analyses.

Accordingly, the present sampling design supports comparison among the investigated FGD streams and plant materials during the corresponding sampling campaigns, but it is not intended to represent the full long-term temporal variability of either power plant.

Prior to laboratory analyses, the FGD gypsum samples were dried at 45 °C to constant mass and homogenized by manual grinding in a mortar, following the established sample preparation procedures for FGD gypsum characterization. This pretreatment was applied to the samples used for physicochemical characterization, sequential extraction, and aqueous leaching experiments. The same initial preparation conditions were applied to the samples used for XRD analysis. Additional portions of FGD-A, FGD-B, and FGD-C were subsequently heated at 105 °C.

Particle-size distributions of all three FGD gypsum materials were determined by laser diffraction using an ANALYSETTE 22 NeXT particle-size analyzer (FRITSCH, GmbH, Idar-Oberstein, Germany). FGD-A exhibited D10, D50 (median particle diameter), and D95 (particle diameter below which 95% of particles are smaller) values of 0.35, 4.3, and 22.5 µm, respectively, while FGD-B exhibited corresponding values of 0.31, 3.2, and 17.0 µm, respectively. FGD-C exhibited representative D10, D50, and D95 values of 15, 45, and 142.5 µm, respectively, indicating a considerably coarser particle-size distribution than FGD-A and FGD-B.

2.2. Physicochemical and Compositional Characterization of FGD Gypsum

The physicochemical and bulk compositional characteristics of the investigated FGD gypsum samples were determined using standardized gravimetric, titrimetric, chromatographic, spectrometric, and X-ray fluorescence procedures. The analytical methods and instrumentation are summarized in Table 2. The scope of physicochemical analyses differed among the investigated materials according to the specific requirements of the corresponding industrial measurement campaigns.

Table 2. Analytical methods and instruments used for physicochemical and compositional characterization of FGD gypsum.

Parameter	Analytical Method	Instrument/Equipment
$CaSO_4 \cdot 2H_2O$	VGB-M 701e:2008 [26]; ASTM C 471M:2020 [27]	Analytical balance, Sartorius Lab Instruments GmbH & Co. KG, Göttingen, Germany and drying oven IKA Werke GmbH & Co. KG, Staufen, Germany

Table 2. *Cont.*

Parameter	Analytical Method	Instrument/Equipment
Free moisture	VGB-M 701e:2008 [26]; ASTM C471M-20 [27]	Analytical balance, Sartorius Lab Instruments GmbH & Co. KG, Göttingen, Germany and drying oven IKA Werke GmbH & Co. KG, Staufen, Germany
Water-soluble MgO, Na_2O	EN ISO 11885:2011 [28]; ICP-OES	iCAP PRO XP Duo ICP-OES spectrometer, Thermo Fisher Scientific, Bremen, Germany
Cl^-	EN ISO 10304-1:2009 [29]; ion chromatography	Dionex Aquion ion chromatograph, Thermo Fisher Scientific, Waltham, MA, USA
$CaSO_3 \cdot 0.5H_2O$	Standard Method 4500-SO_3^{2-} B [30]; iodometric titration	Digital burette, BRAND GMBH + CO KG, Wertheim, Germany
pH	EN ISO 10390:2022 [31]	Orion Star A221 pH meter, Thermo Fisher Scientific, Waltham, MA, USA
CaO, SO_3	X-ray fluorescence analysis	EDXRF 2000 spectrometer, Oxford Instruments, High Wycombe, United Kingdom
CO_2, $Ca(OH)_2$, combined water, free CaO	Gravimetric and thermal analysis	Analytical balance, KERN & SOHN GmbH, Balingen, Germany; drying oven, BINDER, GmbH, Tuttlingen, Germany; laboratory furnace, Mazzali, Paderno Dugnano, Italy

2.3. X-Ray Diffraction Analysis

Powder X-ray diffraction (XRD) measurements were performed using a Rigaku Ultima IV diffractometer (Rigaku Corporation, Tokyo, Japan) operated at 40 kV and 40 mA, using Cu Kα radiation. Diffraction patterns were recorded over the 2θ range of 5–70° with a step width of 0.020° at a scanning rate of 10° min^{-1}. Phase identification was based on characteristic diffraction reflections and comparison with the corresponding International Centre for Diffraction Data (ICDD) PDF-2 reference patterns, supported by published XRD data for gypsum and calcium sulfate hemihydrate [32,33]. XRD measurements were performed before and after heating at 105 °C to evaluate changes in crystalline phase composition and diffraction characteristics.

2.4. Sequential Extraction of Trace Elements

A four-step sequential extraction procedure was applied to the three FGD gypsum samples in duplicate, using approximately 1.00 g of sample. The procedure was based on the general operational principles of sequential extraction described by Tessier et al. [20] and the BCR framework refined by Rauret et al. [21] but was modified with respect to the extraction reagents and conditions used in the present study. The exact extraction conditions are summarized in Table 3.

The reagents used for sequential extraction included acetic acid (Honeywell Fluka, Seelze, Germany), hydroxylamine hydrochloride (Merck, Darmstadt, Germany), ammonium acetate (Merck, Darmstadt, Germany), hydrogen peroxide (Supelco, Darmstadt, Germany), nitric acid (Fisher Chemical, Loughborough, UK), and hydrochloric acid (Fisher Chemical, Loughborough, UK).

The contribution of each fraction was calculated relative to the sum of all four sequentially recovered fractions and expressed as a percentage. For comparative purposes, F1–F3 were combined as the operationally non-residual fraction, while F4 was treated as the residual fraction. These terms describe extraction-defined pools and are not direct measures of environmental mobility.

Table 3. Sequential extraction procedure applied to FGD gypsum samples.

Fraction	Operationally Defined Fraction	Extraction Reagent	Extraction Conditions	Post-Treatment
F1	Acid-soluble/ exchangeable	40 mL 0.11 M CH_3COOH	16 h, 40 rpm, 26 °C	Centrifugation, 3000 rpm, 20 min; residue washed with 20 mL DI water
F2	Reducible	40 mL 0.5 M $NH_2OH{\cdot}HCl$; pH adjusted to ≈1.5 with 2 M HNO_3	16 h, 40 rpm, 26 °C	Centrifugation, 3000 rpm, 20 min; residue washed with 20 mL DI water
F3	Oxidizable	2 × 10 mL 8.8 M H_2O_2, followed by 50 mL 1 M NH_4CH_3COO; pH ≈ 2 with HNO_3	H_2O_2 treatment at ≈90 °C; NH_4CH_3COO extraction: 16 h, 40 rpm, 27 °C	Centrifugation, 3000 rpm, 20 min; residue washed with 20 mL DI water
F4	Residual	Aqua regia: 7.0 mL concentrated HCl + 2.3 mL concentrated HNO_3	80–90 °C to dryness	20 mL 0.5% HNO_3, 1 h; filtration through 0.22 µm nylon filter

Note: F1—acid-soluble/exchangeable fraction; F2—reducible fraction; F3—oxidizable fraction; F4—residual fraction; DI—deionized.

For independent total trace-element determination, duplicate aliquots (0.100 g) of each homogenized FGD gypsum material were subjected to microwave-assisted digestion using 8 mL of HNO_3 (70%, Fisher Chemical, Loughborough, UK) and 2 mL of HF (49%; Centrohem, Belgrade, Serbia) in an MPS 320 microwave digestion system (PerkinElmer, Shelton, CT, USA) equipped with MR-50 vessels. The digestion program consisted of heating to 160 °C (5 min ramp, 5 min hold), followed by heating to 210 °C (3 min ramp, 40 min hold). After cooling, 12 mL of H_3BO_3 solution (5 g per 100 mL of water; CARLO ERBA Reagents, Val-de-Reuil, France) was added, followed by a second microwave-assisted treatment at 190 °C (5 min ramp, 10 min hold) to complex residual fluoride. Following the second microwave-assisted treatment, the digestates were quantitatively transferred and diluted to a final volume of 50 mL. An aliquot of each digestate was subsequently diluted fivefold for ICP-MS analysis. Total concentrations were calculated using the individual sample masses, final digestate volume, and dilution factor.

Sequential-extraction recovery was calculated for each element as R (%) = (ΣF1–F4/TC) × 100, where ΣF1–F4 represents the sum of concentrations recovered in the four extraction fractions and TC is the independently determined total concentration obtained by microwave-assisted digestion.

2.5. Aqueous Leaching Test

A batch aqueous leaching test was performed using 10 g of FGD gypsum and 100 mL of deionized water, corresponding to a liquid-to-solid ratio of 10 L kg^{-1}. The suspensions were agitated for 24 h at 120 rpm, centrifuged at 3000 rpm for 20 min, and filtered through a 0.45 µm membrane filter. The leachates were analyzed for pH, electrical conductivity, sulfate, chloride, and trace elements. pH and electrical conductivity were measured using a Wissenschaftlich-Technische Werkstätten (WTW) multiparameter instrument (Xylem Analytics Germany GmbH, Weilheim, Germany). Sulfate and chloride were determined by ion chromatography using a Dionex Aquion ion chromatograph (Thermo Fisher Scientific, Waltham, MA, USA). Trace elements were determined by inductively coupled plasma mass spectrometry using a NexION 1000 ICP-MS (PerkinElmer, Shelton, CT, USA). The test was used as a direct short-term measure of aqueous release and interpreted independently from the sequential-extraction fractions.

2.6. ICP-MS Analysis and Quality Assurance

Trace-element concentrations in the sequential-extraction solutions, aqueous leachates and independently digested samples were determined by inductively coupled plasma mass spectrometry using a NexION 1000 ICP-MS (PerkinElmer, Shelton, CT, USA) equipped with an S23 autosampler (PerkinElmer, Shelton, CT, USA). Measurements were performed in helium kinetic-energy-discrimination mode. The monitored isotopes included ^{75}As, ^{111}Cd, ^{52}Cr, ^{51}V, ^{208}Pb, ^{63}Cu, ^{66}Zn, ^{60}Ni, ^{59}Co and ^{121}Sb.

External calibration was performed using five calibration standards over the concentration range of 0.1–100 μg L^{-1}, with coefficients of determination (R^2) ranging from 0.99716 to 0.99998. Analytical quality control included routine calibration verification using control solutions at 2 and 5 μg L^{-1}, duplicate determinations, and monitoring of analytical performance using control charts. The verified limits of detection (LOD) and quantification (LOQ) ranged from 0.005 to 0.060 μg L^{-1} and from 0.017 to 0.199 μg L^{-1}, respectively, depending on the element. Results below the applicable detection limit were reported as <LOD.

Sequential extraction and aqueous leaching experiments were performed in duplicate (n = 2) for each representative homogenized FGD gypsum material, and results were reported as mean values. Agreement between duplicate determinations was assessed using the relative percent difference (RPD).

Because duplicate sequential-extraction and aqueous-leaching measurements represent technical replicates of one representative homogenized sample per FGD material, inferential statistical comparisons among FGD-A, FGD-B, and FGD-C were not considered appropriate.

3. Results and Discussion

3.1. Physicochemical, Compositional and Mineralogical Characteristics

The physicochemical and bulk compositional characteristics of the investigated FGD gypsum materials are summarized in Table 4. Differences in gypsum quality among full-scale wet-FGD installations have also been reported by Hansen et al. [34]. FGD-A and FGD-B exhibited comparable characteristics, with $CaSO_4 \cdot 2H_2O$ contents exceeding 98.6 wt.% and low concentrations of chloride, water-soluble MgO and Na_2O, and residual $CaSO_3 \cdot 0.5H_2O$. In contrast, FGD-C exhibited a lower gypsum content (87.47–92.06 wt.%). Additional compositional parameters were determined for FGD-C according to the specific requirements of the corresponding industrial measurement campaign.

Table 4. Physicochemical and bulk compositional characteristics of the investigated FGD gypsum materials.

Parameter	FGD-A	FGD-B	FGD-C
$CaSO_4 \cdot 2H_2O$ (wt.%)	98.64–98.90	98.61–98.81	87.47–92.06
Free moisture (wt.%)	8.99–9.87	8.08–9.57	5.25–8.57
pH	6.92–7.46	7.29–7.60	7.35–7.80
Chloride, Cl^- (wt.%)	0.004–0.008	0.008–0.009	0.008–0.009
Water-soluble MgO (wt.%)	0.001–0.003	0.006–0.016	0.009–0.018
Water-soluble Na_2O (wt.%)	0.001–0.002	≈0.003	0.002–0.004
$CaSO_3 \cdot 0.5H_2O$ (wt.%)	0.097–0.388	0.032–0.127	0.024–0.118
CaO (wt.%)	32.12–32.21	32.11–32.18	29.84–31.60
SO_3 (wt.%)	45.87–45.99	45.85–45.95	40.66–42.77

Table 4. *Cont.*

Parameter	FGD-A	FGD-B	FGD-C
Combined water (wt.%)	20.65–20.70	20.64–20.68	17.62–20.20
CO_2 (wt.%)	ND	ND	0.10–0.30
$Ca(OH)_2$ (wt.%)	ND	ND	0.037–0.130
Free CaO (wt.%)	ND	ND	1.10–2.05

Note: Values are presented as ranges of the available measurements. ND—not determined. Additional compositional analyses (CaO, SO_3, combined water, CO_2, $Ca(OH)_2$, and free CaO) were performed for FGD-C according to the specific requirements of the corresponding industrial measurement campaign.

XRD analysis (Figure 1) showed that gypsum ($CaSO_4 \cdot 2H_2O$) was the predominant crystalline phase in all three investigated FGD materials (FGD-A, FGD-B, and FGD-C). The diffraction patterns exhibited sharp and well-defined reflections, indicating a high degree of crystallinity. Characteristic gypsum reflections were identified at 2θ values of approximately 11.60°, 20.69°, 23.35°, 29.08°, 31.07°, and 33.33°, together with additional reflections at higher diffraction angles. These reflections were consistent with the reference pattern for gypsum and published XRD data for FGD-derived gypsum [32].

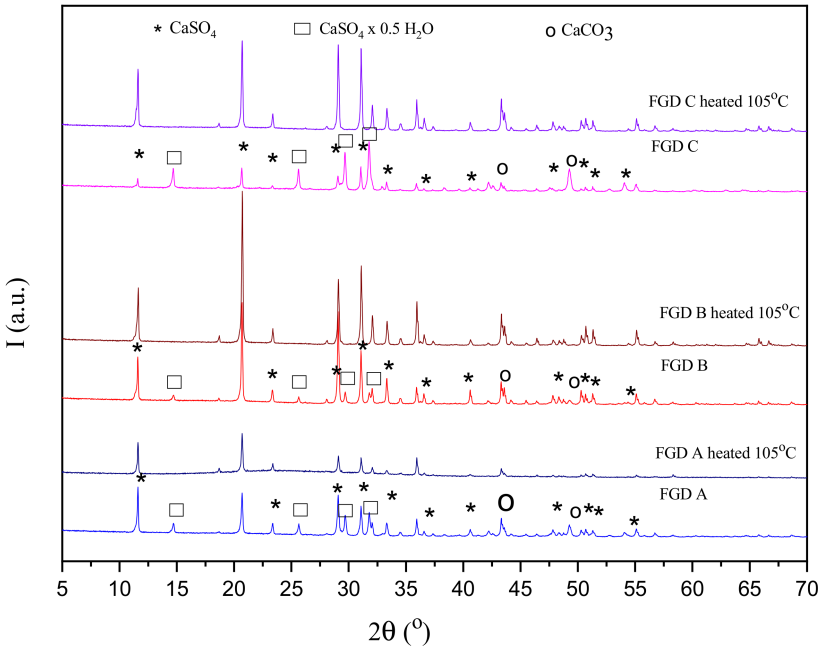


Figure 1. XRD patterns of FGD-A, FGD-B, and FGD-C before and after heating at 105 °C. The identified crystalline phases are gypsum ($CaSO_4 \cdot 2H_2O$), calcium sulfate hemihydrate ($CaSO_4 \cdot 0.5H_2O$; □), anhydrite ($CaSO_4$; *), and calcite ($CaCO_3$; ○). The diffraction patterns are vertically offset for clarity.

In addition to gypsum, calcium sulfate hemihydrate ($CaSO_4 \cdot 0.5H_2O$), anhydrite ($CaSO_4$), and calcite ($CaCO_3$) were identified as accompanying crystalline phases. The identification of calcium sulfate hemihydrate was supported by characteristic diffraction reflections and published investigations of calcium sulfate hemihydrate [32,33]. Differences in the relative intensities of the diffraction reflections were observed among FGD-A, FGD-B, and FGD-C, indicating variations in their crystalline characteristics. The occurrence of calcite is consistent with the use of limestone as a sorbent in wet flue gas desulfurization systems, including the installation at Kostolac B [35].

Comparison of the diffraction patterns before and after heating at 105 °C revealed changes in the characteristic reflections of the calcium sulfate phases in all three FGD

materials (Figure 1). Following heating, the diffraction maximum assigned to calcium sulfate hemihydrate disappeared in FGD-A, FGD-B, and FGD-C, whereas the characteristic reflections of anhydrite remained observable. Changes in the relative intensities of the anhydrite reflections were also observed. These observations are consistent with the temperature-dependent behavior of calcium sulfate phases reported in studies of FGD gypsum dehydration [36].

The observed differences indicate heat-induced changes in the crystalline phase composition of the investigated FGD gypsum materials. The redistribution of relative diffraction intensities may be associated with changes in phase contributions and/or crystallographic preferred orientation. However, the extent of these changes cannot be quantified from the present qualitative XRD results alone. These mineralogical changes may be relevant to subsequent processing and environmental behavior, although their effects on trace-element leaching were not directly investigated in the present study.

3.2. Sequentially Recovered Trace-Element Concentrations

The concentrations summed across the four sequential-extraction fractions (ΣF1–F4) were used to compare the overall sequentially recovered trace-element concentrations among the samples (Table 5).

Table 5. Cumulative sequentially recovered trace-element concentrations (ΣF1–F4) in FGD-A, FGD-B, and FGD-C.

Element	FGD-A (mg kg^{-1})	FGD-B (mg kg^{-1})	FGD-C (mg kg^{-1})
As	42.249 ± 5.467	33.512 ± 0.237	16.694 ± 0.178
Cd	0.441 ± 0.020	0.364 ± 0.010	0.261 ± 0.011
Cr	3.723 ± 0.435	2.715 ± 0.054	15.573 ± 0.216
Pb	3.469 ± 0.409	3.104 ± 0.404	1.423 ± 0.223
Cu	2.291 ± 0.063	1.426 ± 0.158	1.779 ± 0.001
Ni	15.173 ± 0.831	9.323 ± 0.985	3.427 ± 0.201
V	2.580 ± 0.068	2.408 ± 0.059	4.323 ± 0.014
Zn	16.082 ± 1.757	12.194 ± 2.067	9.578 ± 0.098
Sb	1.091 ± 0.051	1.077 ± 0.194	0.978 ± 0.176
Co	0.690 ± 0.018	0.446 ± 0.035	0.277 ± 0.002

Values are reported as mean ± SD of duplicate sequential extractions (n = 2 analytical replicates). Reported concentrations represent the sum of the four sequentially extracted fractions (ΣF1–F4) and should not be interpreted as independently determined total concentrations.

As and Ni concentrations were higher in FGD-A and FGD-B than in FGD-C, whereas Cr showed the opposite pattern and was approximately four- to six-fold higher in FGD-C. V concentrations were also highest in FGD-C. Similar plant-to-plant variability in trace-element concentrations has been reported for FGD gypsum from different coal-fired power plants [15]. Differences in coal-derived particulate inputs and trace-element transfer through air-pollution-control systems may contribute to this variability [18]. The observed differences may also reflect variations in coal composition, fly-ash carry-over, limestone sorbent chemistry, and wet-FGD operating conditions [3,16,18,23]. Although some limestone composition data were available for the Kostolac B power plant from previous measurement campaigns, directly comparable trace-element composition data for coal, fly ash, and limestone from the investigated FGD systems were not available. Therefore, the individual contributions of feed-material composition and operating conditions to the observed differences in FGD gypsum chemistry could not be quantitatively distinguished.

To assess the mass balance of the sequential-extraction procedure, ΣF1–F4 was compared with independently determined total trace-element concentrations obtained by microwave-assisted digestion of the same representative homogenized materials. The corresponding recoveries are presented in Table 6.

Table 6. Independently determined total trace-element concentrations and sequential-extraction recoveries.

Element	FGD-A TC	Recovery (%)	FGD-B TC	Recovery (%)	FGD-C TC	Recovery (%)
As	39.62 ± 0.88	106.6	29.95 ± 0.72	111.9	18.10 ± 0.12	92.3
Cd	0.405 ± 0.010	108.9	0.340 ± 0.026	107.2	0.256 ± 0.013	102.0
Cr	4.34 ± 0.35	85.8	2.75 ± 0.14	98.8	14.21 ± 0.52	109.6
Pb	3.20 ± 0.08	108.4	2.81 ± 0.08	110.5	1.53 ± 0.06	92.9
Cu	2.04 ± 0.05	112.2	1.40 ± 0.08	102.1	1.69 ± 0.05	105.4
Ni	15.15 ± 0.56	100.1	8.82 ± 0.24	105.7	3.76 ± 0.12	91.0
V	2.39 ± 0.09	108.0	2.21 ± 0.07	109.2	4.35 ± 0.15	99.3
Zn	17.36 ± 2.29	92.6	12.87 ± 1.02	94.8	8.89 ± 0.49	107.7
Sb	1.062 ± 0.041	102.7	0.942 ± 0.014	114.3	0.890 ± 0.044	109.9
Co	0.738 ± 0.006	93.4	0.398 ± 0.020	112.1	0.252 ± 0.009	110.1

Note: TC values are expressed as mean ± SD (mg kg^{-1}) from duplicate independent microwave-assisted digestions (n = 2). Sequential-extraction recovery (%) was calculated as (ΣF1–F4/TC) × 100 using the corresponding mean concentrations. Repeated instrumental measurements of the same digests were not treated as additional independent replicates.

Sequential-extraction recoveries ranged from 85.8% to 114.3% across the three FGD materials, indicating generally reasonable agreement between the sum of the sequentially extracted fractions and independently determined total concentrations.

3.3. Sequential Fractionation and Geochemical Stability of Trace Elements

Sequential extraction revealed pronounced element-specific differences (Figures 2–4). The percentage distributions are presented as mean values with standard deviations calculated from duplicate sequential extractions (n = 2). As, Cd and V showed the strongest non-residual behavior: F1–F3 accounted for approximately 74.4%–82.8% of As, 91.9%–95.4% of Cd and 89.9%–96.8% of V. In contrast, Sb was predominantly residual, with approximately 81.5%–88.3% retained in F4. Cr, Pb, Cu, Zn and Co showed intermediate but generally substantial non-residual contributions, whereas Ni displayed the strongest sample dependence.

Comparison of Figures 2–4 shows that, despite the generally similar element-specific fractionation patterns, the relative contributions of individual fractions varied among FGD-A, FGD-B and FGD-C. The present As and Cd fractionation differs from some published FGD-gypsum systems. Yan et al. [23] reported As and Cd as predominantly residual in their samples, whereas Hao et al. [15] and Zhao et al. [16] also demonstrated that fractionation patterns vary strongly among plants and elements. Such differences reinforce the importance of material-specific characterization rather than assigning a universal mobility pattern to FGD gypsum.

The contrast between As and Sb is particularly notable. Although both elements commonly occur as oxyanion-forming metalloids, their environmental partitioning can differ substantially because of differences in oxidation state, aqueous speciation, and mineral-surface interactions. Previous studies have shown that total trace-element concentration alone does not adequately describe environmental behavior because chemical speciation and solid-phase association can differ markedly among elements [16,17]. More recent investigations of FGD gypsum similarly demonstrate that operational fractionation and leaching behavior are strongly element-dependent [22,23]. In addition, recent studies have

shown that As and Sb can exhibit different adsorption and surface-complexation behavior on Fe- and Al-bearing mineral phases, with their retention also influenced by pH, redox conditions, and co-existing ions [37,38]. These differences provide a plausible explanation for the contrasting operational fractionation observed here, with As predominantly recovered in F1–F3 and Sb largely retained in F4. However, the sequential-extraction data alone do not allow specific host phases or oxidation states to be identified, and dedicated spectroscopic or speciation analyses would be required for such attribution. The contrasting behavior of the investigated elements may also be influenced by their aqueous speciation and pH-dependent interactions with mineral surfaces. Arsenic can occur as arsenite or arsenate species, whose sorption onto Fe- and Al-bearing phases depends on pH, oxidation state, and competing anions [37]. In contrast, cationic metals such as Pb, Cd, Cu, and Zn may be retained through surface adsorption, complexation, or association with secondary mineral phases, while precipitation as hydroxides or carbonates may contribute under favorable chemical conditions [39]. The neutral to slightly alkaline pH of the leachates (7.26–8.16) may influence these processes, although pH alone is insufficient to establish specific retention mechanisms [37,39]. These explanations remain tentative because oxidation-state speciation, reactive surface phases, and mineral saturation conditions were not independently determined.

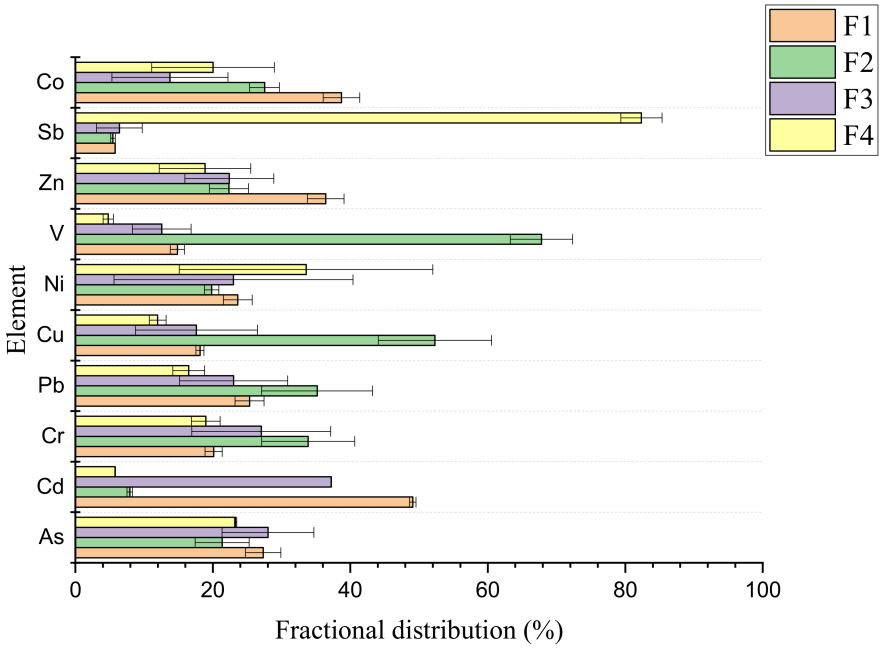


Figure 2. Distribution of trace elements among sequential-extraction fractions (F1–F4) in FGD-A. Bars show mean values ± SD (n = 2).

3.4. Aqueous Leaching Characteristics

The aqueous leaching test provided direct information on short-term release under identical water-contact conditions. The leachates were neutral to slightly alkaline, with pH values ranging from 7.26 to 8.16, while electrical conductivity varied within a relatively narrow range of 2.43–2.83 mS cm^{-1} (Table 7). Sulfate concentrations were also comparable among the three materials, ranging from 1533.8 to 1726.4 mg L^{-1}, indicating broadly similar dissolution of the sulfate matrix under the applied test conditions.

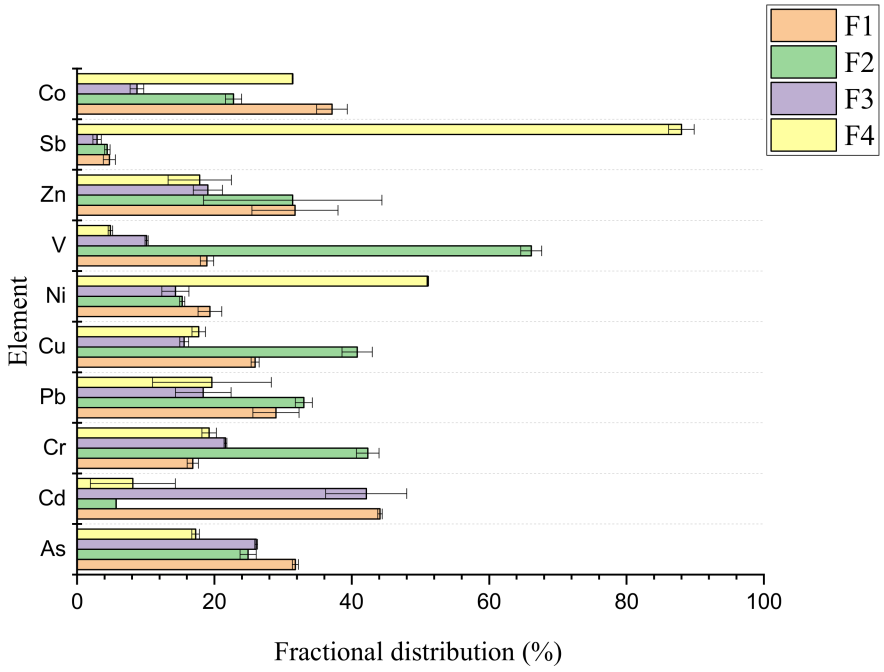


Figure 3. Distribution of trace elements among sequential-extraction fractions (F1–F4) in FGD-B. Bars show mean values ± SD (n = 2).

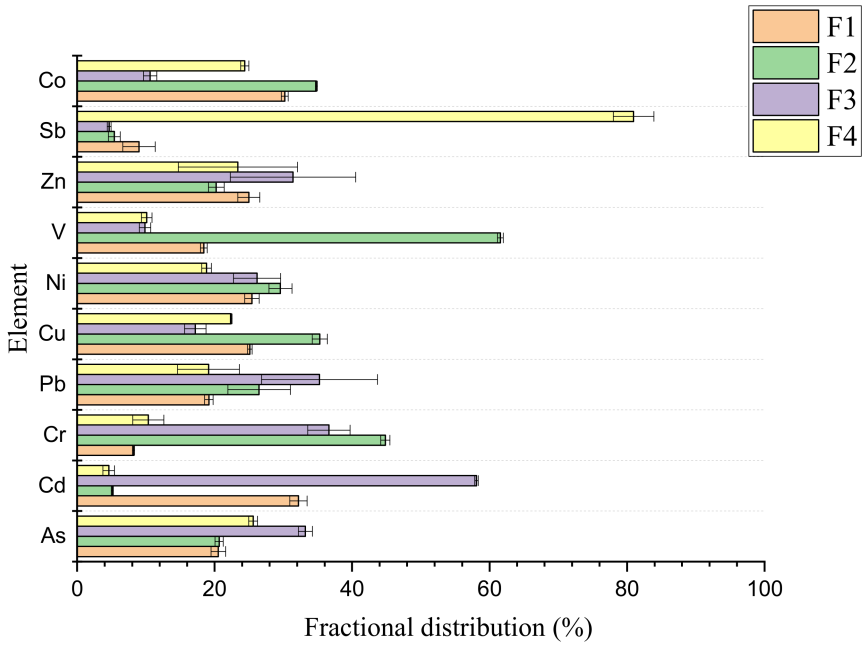


Figure 4. Distribution of trace elements among sequential-extraction fractions (F1–F4) in FGD-C. Bars show mean values ± SD (n = 2).

Table 7. Physicochemical characteristics of aqueous leachates from FGD-A, FGD-B and FGD-C.

Parameter	FGD-A	FGD-B	FGD-C
pH	8.16	7.59	7.26
Electrical conductivity (mS cm^{-1})	2.65	2.83	2.43
SO_4^{2-} (mg L^{-1})	1533.8	1726.4	1663.6
Cl^- (mg L^{-1})	28.15	27.95	7.75

Chloride showed a more pronounced sample-related difference. FGD-A and FGD-B produced nearly identical concentrations of 28.15 and 27.95 mg L^{-1}, respectively, whereas FGD-C released only 7.75 mg L^{-1}. Thus, despite relatively similar sulfate concentrations and electrical conductivity, the chloride concentration differed markedly between FGD-C and the two other materials.

Trace-element release was generally low but clearly sample- and element-dependent (Table 8). FGD-B showed the highest dissolved As (2.41 µg L^{-1}) and Cd (1.12 µg L^{-1}) concentrations and, most notably, a Zn concentration of 5.25 µg L^{-1}, approximately eleven times higher than that measured for FGD-A. FGD-A showed the highest Cr (0.19 µg L^{-1}), Cu (0.15 µg L^{-1}) and Ni (1.19 µg L^{-1}) concentrations, although the Ni concentration in FGD-B was very similar (1.14 µg L^{-1}). In contrast, FGD-C exhibited the highest V (0.98 µg L^{-1}) and Sb (0.46 µg L^{-1}) concentrations. Co concentrations were low in all three leachates, ranging from 0.07 to 0.19 µg L^{-1}, while Pb remained below the validated detection limit in all samples.

Table 8. Mean trace-element concentrations in aqueous leachates.

Element	FGD-A (µg L^{-1})	FGD-B (µg L^{-1})	FGD-C (µg L^{-1})
As	1.99	2.41	0.82
Cd	0.62	1.12	0.40
Cr	0.19	0.08	0.08
V	0.61	0.58	0.98
Pb	<LOD	<LOD	<LOD
Cu	0.15	0.07	0.08
Zn	0.46	5.25	0.97
Ni	1.19	1.14	0.58
Co	0.17	0.19	0.07
Sb	0.41	0.37	0.46

Values represent means of duplicate leaching experiments (n = 2). Pb concentrations were below the detection limit (LOD = 0.041 µg L^{-1}).

The relatively similar sulfate concentrations, together with the distinctly different release patterns of individual trace elements, indicate that trace-element release was not controlled solely by the overall extent of gypsum dissolution. Previous studies have shown that constituent release from FGD gypsum is strongly influenced by the applied leaching conditions [24]. Longer-term or management-scenario assessments may also produce different release estimates from conventional short-term procedures [25]. Element-specific differences between chemical occurrence forms and aqueous release have likewise been observed in recent FGD-gypsum studies [23].

3.5. Relationship Between Sequential Fractionation and Aqueous Release

Comparison of the operationally defined non-residual fraction (F1 + F2 + F3) with aqueous trace-element concentrations showed no simple one-to-one relationship between solid-phase fractionation and short-term aqueous release (Figures 5–7). As and Cd exhibited high non-residual contributions together with measurable aqueous concentrations, although the magnitude of release was not proportional to the non-residual percentage alone. V was also predominantly associated with the non-residual fractions in all three samples, but its highest aqueous concentration was observed in FGD-C. In contrast, Sb was predominantly retained in the residual fraction (F4), while measurable and relatively similar Sb concentrations were observed in the leachates of all three materials.

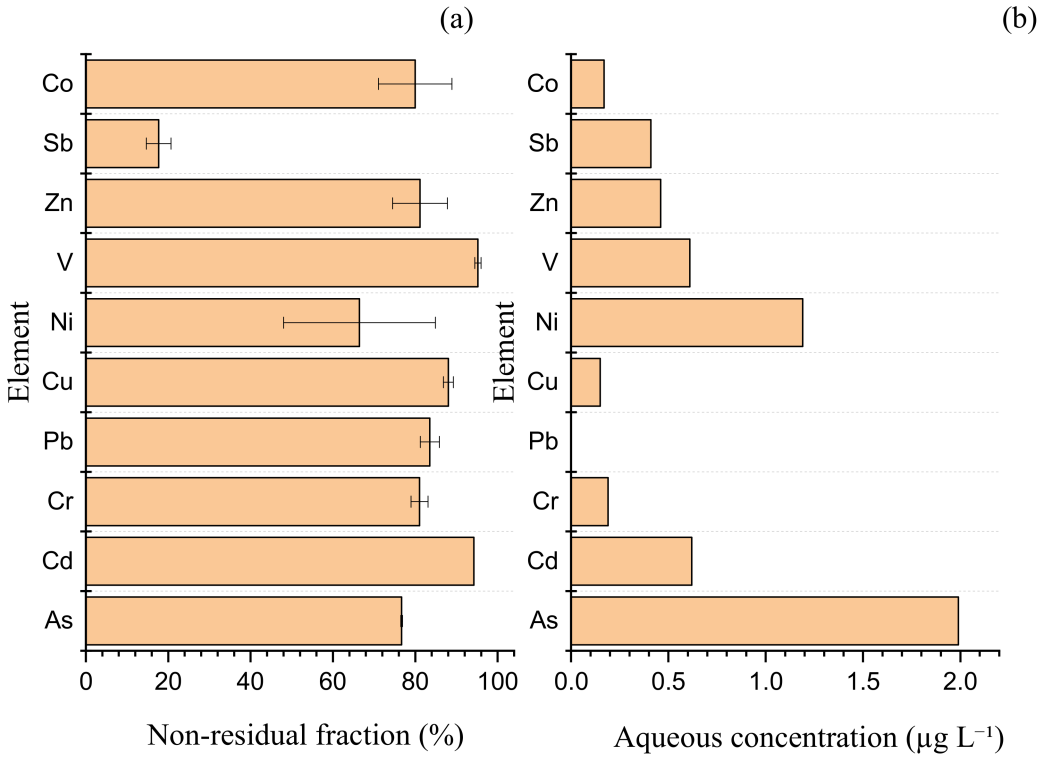


Figure 5. Comparison of (**a**) non-residual fractions (F1–F3, %) and (**b**) aqueous trace-element concentrations (μg L^{-1}) in FGD-A. Error bars in (**a**) represent SD of duplicate sequential extractions (n = 2).

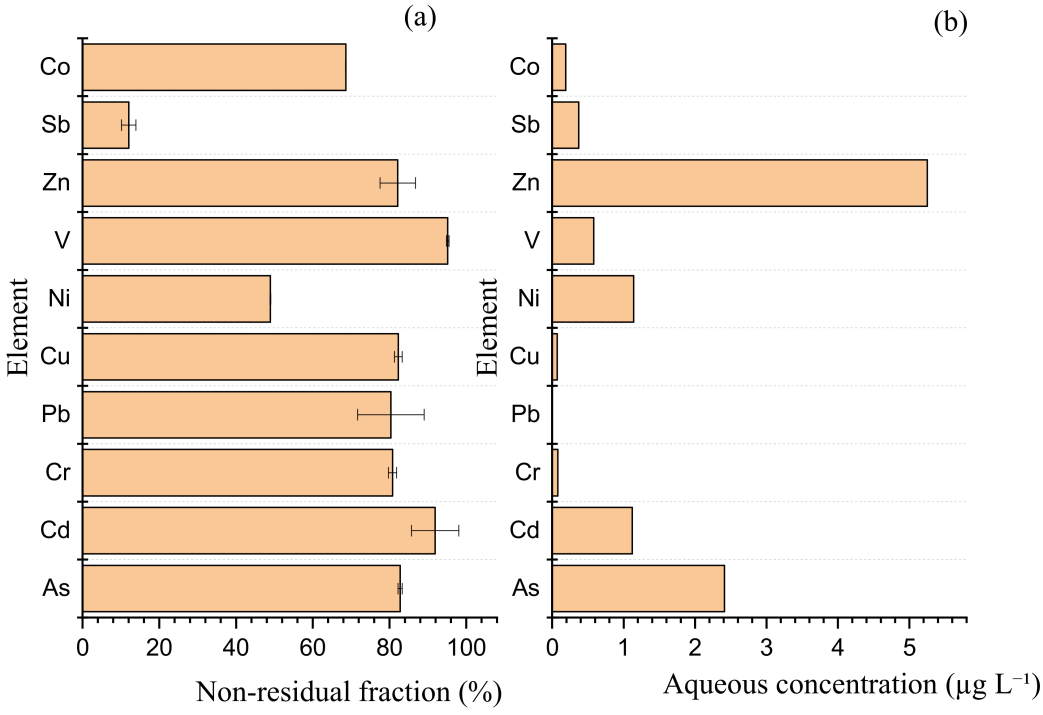


Figure 6. Comparison of (**a**) non-residual fractions (F1–F3, %) and (**b**) aqueous trace-element concentrations (μg L^{-1}) in FGD-B. Error bars in (**a**) represent SD of duplicate sequential extractions (n = 2).

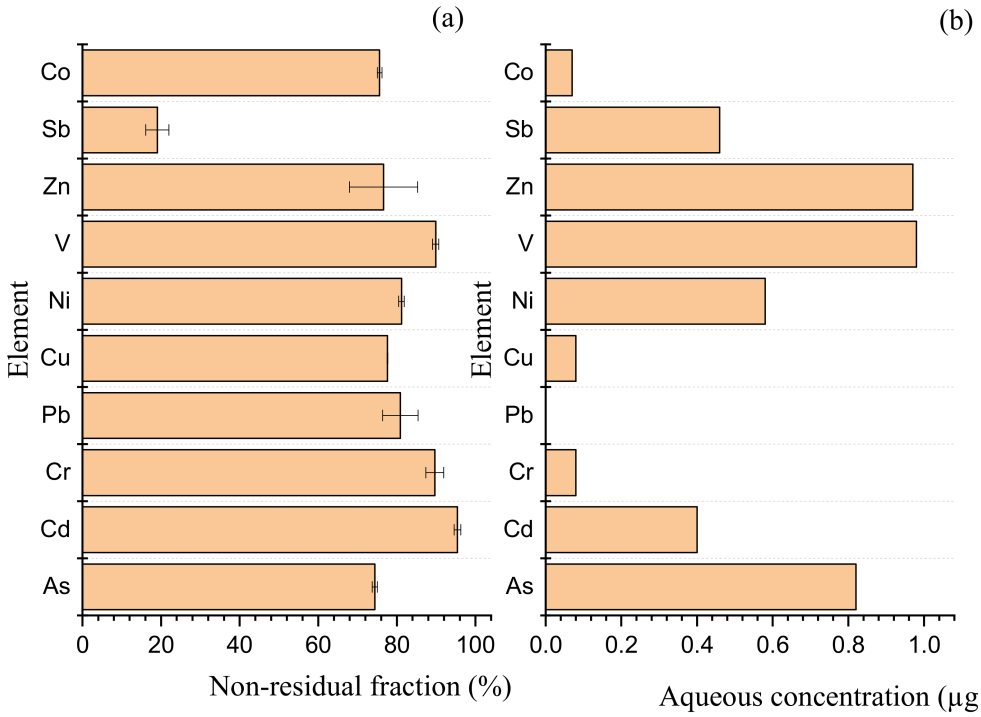


Figure 7. Comparison of (**a**) non-residual fractions (F1–F3, %) and (**b**) aqueous trace-element concentrations (μg L^{-1}) in FGD-C. Error bars in (**a**) represent SD of duplicate sequential extractions (n = 2).

The comparison of Figures 5–7 further illustrates that similar non-residual contributions can correspond to markedly different aqueous concentrations. This distinction is particularly evident for Pb. Despite appreciable contributions of F1–F3 in all three materials, Pb remained below the validated detection limit in the corresponding aqueous leachates. Thus, the operationally defined non-residual fraction should not be interpreted as a direct measure of water leachability.

Zn provides another clear example. Although its non-residual contribution was broadly comparable among the three FGD materials, the aqueous Zn concentration in FGD-B (5.25 μg L^{-1}) was substantially higher than those measured for FGD-A (0.46 μg L^{-1}) and FGD-C (0.97 μg L^{-1}). Similarly, V showed high non-residual contributions in all samples, whereas its aqueous concentration was highest in FGD-C. Conversely, Sb was predominantly associated with F4, yet low but measurable aqueous concentrations were detected in all three leachates.

These differences reflect the fundamentally different information provided by the two experimental approaches. Sequential extraction describes operationally defined solid-phase associations, whereas aqueous leaching directly measures release under specified water-contact conditions.

Unlike sequential extraction, which employs reagents with different acidity, complexation capacity, and oxidation–reduction conditions, aqueous leaching was performed using deionized water under near-neutral to slightly alkaline conditions. Consequently, the release of individual elements may be controlled by their aqueous speciation, solubility, sorption onto mineral surfaces, and possible formation of secondary precipitates, as well as the duration of water contact. Therefore, elements recovered in non-residual fractions are not necessarily released to the same extent during short-term water leaching.

Chemical speciation has been shown to influence the potential mobility of trace elements in FGD-derived materials [17], while direct release from FGD gypsum is strongly affected by the imposed leaching conditions [24,25]. Recent FGD-gypsum studies also demonstrate that fractionation and leaching responses are element-specific [23]. Sequential

fractionation and aqueous leaching should therefore be interpreted as complementary rather than interchangeable indicators of trace-element behavior.

3.6. Comparison of FGD Gypsum Materials from Different Operating Streams and Power Plants

The within-plant comparison is represented by FGD-A and FGD-B. Both materials had $CaSO_4 \cdot 2H_2O$ contents above 98.6 wt.% and showed closely comparable conventional physicochemical characteristics, yet they differed in sequentially recovered trace-element concentrations, fractionation patterns and aqueous release. FGD-A contained higher sequentially recovered As and Ni concentrations, whereas FGD-B exhibited markedly greater aqueous Zn release. These results demonstrate that similarity in bulk technological characteristics within the same power plant does not necessarily imply identical trace-element behavior. Comparable variability in trace-element concentrations and partitioning has been reported for FGD gypsum from different coal-fired power plants [15].

The corresponding performance-test data (Table 1) also indicate differences in the operating conditions of the C1 and C2 systems, particularly in inlet and outlet SO_2 concentrations and desulfurization efficiency. However, these observations do not establish a direct causal relationship between individual operating parameters and the trace-element behavior of the resulting gypsum materials.

FGD-C contained a lower $CaSO_4 \cdot 2H_2O$ content (87.47–92.06 wt.%) and higher sequentially recovered Cr and V concentrations, but lower As and Ni concentrations, than FGD-A and FGD-B. Its leachate also exhibited a substantially lower chloride concentration and the highest aqueous V concentration. Previous studies have likewise shown that trace-element concentration and operational fractionation can vary considerably among FGD gypsum materials [16]. Differences in coal-derived inputs, sorbent characteristics, and wet-FGD process conditions are among the factors that can contribute to such variability [3,18,23]. In the present study, however, the available dataset does not permit the contribution of individual factors to be distinguished.

Taken together, the gypsum-dominated XRD patterns, relatively similar sulfate release and clearly different trace-element fractionation and aqueous-release behavior indicate that bulk mineralogy alone is insufficient to predict the environmental response of FGD gypsum. Previous investigations have similarly shown that element release depends on chemical association and on the conditions imposed during leaching [17,24,25]. Therefore, differences among FGD gypsum materials originating from separate operating streams and power plants should be considered when representative FGD gypsum materials are selected for environmental assessment, reuse or further processing.

3.7. Implications for Environmental Assessment and Valorization

The increasing interest in FGD gypsum as a secondary raw material has promoted its use and investigation in construction-related applications, mineral carbonation and other valorization pathways [9]. However, assessment based solely on conventional gypsum purity may overlook differences in the distribution and potential release of associated trace elements. The present results illustrate this limitation: FGD-A and FGD-B were high-purity gypsum materials but exhibited different trace-element fractionation and aqueous-release behavior, whereas FGD-C had a lower bulk gypsum content while remaining predominantly gypsum-based according to XRD.

For environmental assessment, sequential extraction provides information on operationally defined element associations within the solid and distinguishes fractions released by progressively more aggressive reagents [20,21]. Direct aqueous leaching, in contrast, evaluates the amount actually released under specified water-contact conditions, and constituent release is sensitive to the applied test conditions [24]. Longer-term or alternative

management scenarios may yield different release patterns [25]. The lack of a simple proportional relationship between the non-residual fraction and aqueous concentrations observed in the present study further demonstrates that the two approaches should be interpreted as complementary rather than interchangeable.

This distinction is particularly important when FGD gypsum is intended for reuse, because processing may alter mineral phases, surface properties and element associations. Recent work on FGD-gypsum-derived construction products has combined technological performance, leaching behavior and life-cycle assessment [14]. Carbonation-based valorization is of particular interest because mineral transformation can alter carbonation efficiency and the partitioning and fate of associated trace elements [13]. Consequently, combining bulk composition, mineralogical characterization, sequential extraction and direct leaching provides a more robust basis for screening FGD gypsum prior to its use in construction materials, carbonation processes or other applications.

Environmental assessment should therefore accompany technological evaluation throughout the selection and processing of FGD gypsum, particularly where physicochemical transformation of the original material is involved. Such an integrated approach is consistent with the broader transition from simple waste utilization toward valorization strategies in which material performance and environmental stability are considered together [9,14].

3.8. Study Limitations

The results should be interpreted within the scope of the investigated sampling campaigns and laboratory conditions. Although repeated time-resolved field sampling was performed for each FGD material, the detailed XRD, sequential-extraction, and aqueous-leaching analyses were conducted on one representative homogenized laboratory sample per material. The duplicate extraction and leaching determinations therefore represent technical replicates and do not provide a basis for inferential assessment of long-term process variability. In addition, the batch leaching test represents a defined short-term water-contact scenario and should not be interpreted as a direct measure of long-term field release. Accordingly, the comparisons reported here are specific to the investigated FGD materials and sampling campaigns and should not be extrapolated to the full temporal variability of the respective power plants. The lack of directly comparable feed-material trace-element composition data further limits the identification of factors responsible for the observed differences among the FGD gypsum materials.

4. Conclusions

The comparative assessment of three Serbian FGD gypsum materials revealed differences in their physicochemical characteristics and trace-element behavior. FGD-A and FGD-B contained >98.6 wt.% $CaSO_4 \cdot 2H_2O$ and showed closely comparable conventional physicochemical characteristics, whereas FGD-C contained 87.47–92.06 wt.% $CaSO_4 \cdot 2H_2O$. XRD confirmed gypsum as the predominant crystalline phase in FGD-A, FGD-B, and FGD-C, accompanied by calcium sulfate hemihydrate, anhydrite, and calcite. Heating at 105 °C resulted in changes in the characteristic diffraction reflections and relative intensities of calcium sulfate phases.

Sequential extraction revealed strongly element-dependent fractionation. As, Cd and V were predominantly associated with the operationally defined non-residual fractions, whereas Sb was mainly retained in the residual fraction. Ni and several other trace elements showed greater sample-dependent variability. Aqueous leaching was generally low but clearly sample- and element-dependent: FGD-B exhibited the highest Zn concentration,

FGD-C the highest V concentration, while Pb remained below the validated detection limit in all leachates.

The proportion of operationally defined non-residual fractions was not directly proportional to aqueous release. This confirms that sequential extraction and water leaching provide complementary rather than interchangeable information on trace-element behavior. The results further demonstrate that even FGD gypsum materials with similar bulk technological characteristics and gypsum-dominated mineralogy can differ substantially in trace-element fractionation and short-term aqueous release.

Accordingly, assessment of FGD gypsum prior to reuse or further processing should integrate bulk composition, mineralogical characterization, operational trace-element fractionation and direct leaching rather than relying on gypsum purity or XRD characteristics alone. The present dataset also provides a baseline for future before–after studies examining how carbonation or mechanochemical processing affects $CaSO_4$ transformation, CO_2 mineralization and the redistribution, retention or release of associated trace elements. Such comparisons will be important for determining whether increased material reactivity can be achieved without adversely affecting environmental stability.

Author Contributions: Conceptualization, S.P.P. and J.I.; methodology, S.P.P., J.I. and I.V.; investigation, S.P.P., J.I. and I.V.; formal analysis, L.M., J.I. and I.V.; validation, T.L. and W.T.; data curation, J.I., I.V. and S.P.P.; writing—original draft preparation, J.I., L.M. and S.P.P.; writing—review and editing, L.M., T.L., W.T. and S.S.; supervision, L.M., S.P.P. and S.S.; project administration, S.P.P. All authors have read and agreed to the published version of the manuscript.

Funding: This research was funded by the Ministry of Science, Technological Development and Innovation of the Republic of Serbia under contract numbers 451-03-33/2026-03/200035 and 451-03-33/2026-03/200017.

Data Availability Statement: The data generated and analyzed during the current study are presented within the article. Additional data are available from the corresponding author upon reasonable request.

Conflicts of Interest: The authors declare no conflicts of interest.

Abbreviations

The following abbreviations are used in this manuscript:

BCR	Community Bureau of Reference
EDXRF	energy-dispersive X-ray fluorescence
FGD	flue gas desulfurization
ICP-MS	inductively coupled plasma mass spectrometry
ICP-OES	inductively coupled plasma optical emission spectrometry
ICDD	International Centre for Diffraction Data
LOD	limit of detection
RPD	relative percent difference
XRD	X-ray diffraction

References

1. Córdoba, P. Status of flue gas desulphurisation (FGD) systems from coal-fired power plants: Overview of the physic-chemical control processes of wet limestone FGDs. *Fuel* **2015**, *144*, 274–286. [CrossRef]
2. Srivastava, R.K.; Jozewicz, W. Flue gas desulfurization: The state of the art. *J. Air Waste Manag. Assoc.* **2001**, *51*, 1676–1688. [CrossRef] [PubMed]
3. Koralegedara, N.H.; Pinto, P.X.; Dionysiou, D.D.; Al-Abed, S.R. Recent advances in flue gas desulfurization gypsum processes and applications—A review. *J. Environ. Manag.* **2019**, *251*, 109572. [CrossRef] [PubMed]

4. Aakriti; Maiti, S.; Jain, N.; Malik, J. A comprehensive review of flue gas desulphurized gypsum: Production, properties, and applications. *Constr. Build. Mater.* **2023**, *393*, 131918. [CrossRef]
5. Liu, S.; Liu, W.; Jiao, F.; Qin, W.; Yang, C. Production and resource utilization of flue gas desulfurized gypsum in China—A review. *Environ. Pollut.* **2021**, *288*, 117799. [CrossRef] [PubMed]
6. Du, J.; Zou, K.; Chen, R.; Zhou, J.; Wang, X.; Zou, Y.; Zhang, Z.; Yang, J. A low-clinker design of ultra-high-performance concrete (UHPC) with high-volume slag activated by flue gas desulfurization (FGD) gypsum. *Constr. Build. Mater.* **2026**, *506*, 144990. [CrossRef]
7. Wan, J.; Deng, H.; Lv, J.; Wang, J. Chloride-free hydrothermal synthesis of high-strength gypsum from flue gas desulfurization (FGD) gypsum. *Surf. Interfaces* **2026**, *80*, 108380. [CrossRef]
8. Wang, L.; Su, L.; Li, M.; Lv, C.; Zhao, W. Synergistic utilization of desulfurization gypsum and flue gas for the sustainable synthesis of nano-$CaCO_3$. *Chem. Eng. J.* **2026**, *534*, 175274. [CrossRef]
9. Moreno, V.; González-Arias, J.; Ruiz-Martinez, J.D.; Balart-Gimeno, R.; Baena-Moreno, F.M.; Leiva, C. FGD-Gypsum Waste to Capture CO_2 and to Recycle in Building Materials: Optimal Reaction Yield and Preliminary Mechanical Properties. *Materials* **2024**, *17*, 3774. [CrossRef] [PubMed]
10. Xu, W.; Liu, C.; Du, K.; Gao, Q.; Liu, Z.; Wang, W. A brief review on flue gas desulfurization gypsum recovery toward calcium carbonate preparation. *Environ. Sci. Adv.* **2024**, *3*, 1351–1363. [CrossRef]
11. Song, K.; Jang, Y.-N.; Kim, W.; Lee, M.G.; Shin, D.; Bang, J.-H.; Jeon, C.W.; Chae, S.C. Precipitation of calcium carbonate during direct aqueous carbonation of flue gas desulfurization gypsum. *Chem. Eng. J.* **2012**, *213*, 251–258. [CrossRef]
12. Wang, B.; Pan, Z.; Du, Z.; Cheng, H.; Cheng, F. Effect of impure components in flue gas desulfurization (FGD) gypsum on the generation of polymorph $CaCO_3$ during carbonation reaction. *J. Hazard. Mater.* **2019**, *369*, 236–243. [CrossRef] [PubMed]
13. Córdoba, P.; Rojas, S. Carbon sequestration through mineral carbonation: Using commercial FGD-gypsum from a copper smelter for sustainable waste management and environmental impact mitigation. *J. Environ. Chem. Eng.* **2024**, *12*, 112510. [CrossRef]
14. Ruiz Martinez, J.D.; Peceño Capilla, B.; Cifuentes Bulté, H.; Leiva, C. Life cycle analysis, leaching, technical and mechanical properties of wallboards composed of flue gas desulfurization gypsum and fly ash with carbon fibers. *Environ. Sci. Pollut. Res.* **2026**, *33*, 13726–13748. [CrossRef] [PubMed]
15. Hao, Y.; Li, Q.; Pan, Y.; Liu, Z.; Wu, S.; Xu, Y.; Qian, G. Heavy metals distribution characteristics of FGD gypsum samples from Shanxi Province 12 coal-fired power plants and its potential environmental impacts. *Fuel* **2017**, *209*, 238–245. [CrossRef]
16. Zhao, S.; Duan, Y.; Lu, J.; Gupta, R.; Pudasainee, D.; Liu, S.; Liu, M.; Lu, J. Thermal stability, chemical speciation and leaching characteristics of hazardous trace elements in FGD gypsum from coal-fired power plants. *Fuel* **2018**, *231*, 94–100. [CrossRef]
17. Al-Abed, S.R.; Jegadeesan, G.; Scheckel, K.G.; Tolaymat, T. Speciation, characterization, and mobility of As, Se, and Hg in flue gas desulphurization residues. *Environ. Sci. Technol.* **2008**, *42*, 1693–1698. [CrossRef] [PubMed]
18. Han, D.; Xu, L.; Wu, Q.; Wang, S.; Duan, L.; Wen, M.; Li, Z.; Tang, Y.; Li, G.; Liu, K. Potential environmental risk of trace elements in fly ash and gypsum from ultra-low emission coal-fired power plants in China. *Sci. Total Environ.* **2021**, *798*, 149116. [CrossRef] [PubMed]
19. Liu, Z.; Hao, Y.; Zhang, J.; Wu, S.; Pan, Y.; Zhou, J.; Qian, G. The characteristics of arsenic in Chinese coal-fired power plant flue gas desulphurisation gypsum. *Fuel* **2020**, *271*, 117515. [CrossRef]
20. Tessier, A.; Campbell, P.G.C.; Bisson, M. Sequential extraction procedure for the speciation of particulate trace metals. *Anal. Chem.* **1979**, *51*, 844–851. [CrossRef]
21. Rauret, G.; López-Sánchez, J.F.; Sahuquillo, A.; Rubio, R.; Davidson, C.; Ure, A.; Quevauviller, P. Improvement of the BCR three step sequential extraction procedure prior to the certification of new sediment and soil reference materials. *J. Environ. Monit.* **1999**, *1*, 57–61. [CrossRef] [PubMed]
22. Sundha, P.; Mukhopadhyay, R.; Basak, N.; Rai, A.K.; Bedwal, S.; Patel, S.; Kumar, S.; Kaur, H.; Chandra, P.; Sharma, P.C.; et al. Characterization of flue gas desulphurized (FGD) gypsum of a coal-fired plant and its relevant risk of associated potential toxic elements in sodic soil reclamation. *Sci. Rep.* **2023**, *13*, 19787. [CrossRef] [PubMed]
23. Yan, K.; Wu, Z.; Li, Z.; Xue, Z.; Guo, Y. Occurrence form and environmental effect of heavy metal in flue gas desulfurization gypsum from Shanxi Province, China. *Environ. Prog. Sustain. Energy* **2025**, *44*, e14597. [CrossRef]
24. Koralegedara, N.H.; Al-Abed, S.R.; Arambewela, M.K.J.; Dionysiou, D.D. Impact of leaching conditions on constituents release from flue gas desulfurization gypsum (FGDG) and FGDG-soil mixture. *J. Hazard. Mater.* **2017**, *324*, 83–93. [CrossRef] [PubMed]
25. Pasini, R.; Walker, H.W. Estimating constituent release from FGD gypsum under different management scenarios. *Fuel* **2012**, *95*, 190–196. [CrossRef]
26. *VGB-M 701e:2008*; Analysis of FGD Gypsum. 2nd ed. VGB PowerTech e.V.: Essen, Germany, 2008.
27. *ASTM C471M-20*; Standard Test Methods for Chemical Analysis of Gypsum and Gypsum Products (Metric). ASTM International: West Conshohocken, PA, USA, 2020. [CrossRef]
28. *SRPS EN ISO 11885:2011*; Water Quality—Determination of Selected Elements by Inductively Coupled Plasma Optical Emission Spectrometry (ICP-OES). Institute for Standardization of Serbia: Belgrade, Serbia, 2011.

29. *SRPS EN ISO 10304-1:2009*; Water Quality—Determination of Dissolved Anions by Liquid Chromatography of Ions—Part 1: Determination of Bromide, Chloride, Fluoride, Nitrate, Nitrite, Phosphate and Sulfate. Institute for Standardization of Serbia: Belgrade, Serbia, 2009.
30. *APHA Method 4500-SO_3^{2-} B*; Sulfite—Determination by Iodometric Method. In Standard Methods for the Examination of Water and Wastewater. American Public Health Association: Washington, DC, USA, 2000.
31. *SRPS EN ISO 10390:2022*; Soil, Treated Biowaste and Sludge—Determination of pH. Institute for Standardization of Serbia: Belgrade, Serbia, 2022.
32. Guan, Q.-J.; Sun, W.; Hu, Y.-H.; Yin, Z.-G.; Guan, C.-P. Synthesis of α-$CaSO_4 \cdot 0.5H_2O$ from flue gas desulfurization gypsum regulated by $C_4H_4O_4Na_2 \cdot 6H_2O$ and NaCl in glycerol-water solution. *RSC Adv.* **2017**, *7*, 27807–27815. [CrossRef]
33. Chen, X.; Wu, Q.; Gao, J.; Tang, Y. Hydration characteristics and mechanism analysis of β-calcium sulfate hemihydrate. *Constr. Build. Mater.* **2021**, *296*, 123714. [CrossRef]
34. Hansen, B.B.; Kiil, S.; Johnsson, J.E. Investigation of the gypsum quality at three full-scale wet flue gas desulphurisation plants. *Fuel* **2011**, *90*, 2965–2973. [CrossRef]
35. Konc Janković, K.; Lazić, D.; Stjepanović, P.; Nešković, J.; Milojković, N. Creation and deposition of gypsum from the desulfurization of TPP Kostolac B flue gas at Drmno open-pit mine. *Bull. Mines* **2022**, *1*, 57–63. [CrossRef]
36. Lou, W.; Guan, B.; Wu, Z. Dehydration behavior of FGD gypsum by simultaneous TG and DSC analysis. *J. Therm. Anal. Calorim.* **2011**, *104*, 661–669. [CrossRef]
37. Xiang, S.; Fu, Z.; Lu, H.; Sun, Y.; Shen, Y.; Wu, F. Antimony and arsenic interactions with iron oxides and aluminum oxides in surface environment: A review focused on processes and mechanisms. *Sci. Total Environ.* **2025**, *979*, 179423. [CrossRef] [PubMed]
38. Kumar, R.; Jing, C.; Yan, L. A critical review on arsenic and antimony adsorption and transformation on mineral facets. *J. Environ. Sci.* **2025**, *153*, 56–75. [CrossRef] [PubMed]
39. Karna, R.R.; Luxton, T.; Bronstein, K.E.; Hoponick Redmon, J.; Scheckel, K.G. State of the science review: Potential for beneficial use of waste by-products for in situ remediation of metal-contaminated soil and sediment. *Crit. Rev. Environ. Sci. Technol.* **2017**, *47*, 65–129. [CrossRef] [PubMed]

Disclaimer/Publisher's Note: The statements, opinions and data contained in all publications are solely those of the individual author(s) and contributor(s) and not of MDPI and/or the editor(s). MDPI and/or the editor(s) disclaim responsibility for any injury to people or property resulting from any ideas, methods, instructions or products referred to in the content.